AGU PUBLICATIONS

Geophysical Research Letters

RESEARCH LETTER
10.1002/2017GL075609

Key Points:
- We provide the highest-resolution heat flux map for Antarctica and its uncertainties
- Our new map represents the subglacial geology much better than previous maps
- This new map will be the base for the future generations of ice sheet model, subglacial hydrology, and sea level change models

Supporting Information:
- Supporting Information S1

Correspondence to:
Y. M. Martos,
yasmina.martos@nasa.gov

Citation:
Martos, Y. M., Catalán, M., Jordan, T. A., Golynsky, A., Golynsky, D., Eagles, G., & Vaughan, D. G. (2017). Heat flux distribution of Antarctica unveiled. *Geophysical Research Letters*, *44*. https://doi.org/10.1002/2017GL075609

Received 12 SEP 2017
Accepted 31 OCT 2017
Accepted article online 6 NOV 2017

Heat Flux Distribution of Antarctica Unveiled

Yasmina M. Martos[1,2,3], Manuel Catalán[4], Tom A. Jordan[1], Alexander Golynsky[5], Dmitry Golynsky[5], Graeme Eagles[6], and David G. Vaughan[1]

[1]British Antarctic Survey (NERC), Cambridge, UK, [2]Now at Department of Astronomy, University of Maryland, College Park, MD, USA, [3]Now at NASA Goddard Space Flight Center, Planetary Magnetospheres Laboratory, Greenbelt, MD, USA, [4]Royal Observatory of the Spanish Navy, San Fernando, Spain, [5]The All-Russia Scientific Research Institute for Geology and Mineral Resources of the Ocean, Saint Petersburg, Russia, [6]Alfred Wegener Institute for Polar and Marine Research, Bremerhaven, Germany

Abstract Antarctica is the largest reservoir of ice on Earth. Understanding its ice sheet dynamics is crucial to unraveling past global climate change and making robust climatic and sea level predictions. Of the basic parameters that shape and control ice flow, the most poorly known is geothermal heat flux. Direct observations of heat flux are difficult to obtain in Antarctica, and until now continent-wide heat flux maps have only been derived from low-resolution satellite magnetic and seismological data. We present a high-resolution heat flux map and associated uncertainty derived from spectral analysis of the most advanced continental compilation of airborne magnetic data. Small-scale spatial variability and features consistent with known geology are better reproduced than in previous models, between 36% and 50%. Our high-resolution heat flux map and its uncertainty distribution provide an important new boundary condition to be used in studies on future subglacial hydrology, ice sheet dynamics, and sea level change.

1. Introduction

Geothermal heat flux depends on several geological factors including heat flux from the mantle, heat production in the crust by radioactive decay, and tectonic history (Pollack et al., 1993). The heat flux underneath the Antarctic Ice Sheet is an important boundary condition for ice sheet behavior and associated sea level change (Golledge et al., 2015) since it keeps basal ice relatively warm, and thus less viscous than colder ice above, and helps supply meltwater at the ice sheet base. This allows for rapid ice flow by sliding over the bed and deformation of the subglacial sediments.

Although heat flux is an important parameter, direct and precise measurements over Antarctica are few, localized and difficult to acquire (Fisher et al., 2015; Hasterok, 2010) since >99% of the continent is covered by ice and the bed can be covered by up to 4 km of ice (Fretwell et al., 2013). Indirect estimates of heat flux derived from temperature profiles in the ice are complicated by frictional heating within the ice and at the ice bed interface as well as the inherited signal from temperature changes over recent and longer glacial time scales (Zagorodnov et al., 2012).

Three main Antarctic-wide heat flux maps have been previously proposed based on satellite magnetic or seismological data (An et al., 2015a; Fox Maule et al., 2005; Shapiro & Ritzwoller, 2004). All were regional estimates derived from low-resolution data showing contradictory and conflicting results. To improve the spatial resolution and the precision of this critical parameter, we derived the first continent-wide heat flux map using airborne magnetic data across Antarctica (Figure 1).

2. Materials and Methods

Our method is based on the fact that ferromagnetic materials retain their magnetism only until reaching the Curie temperature, which is found at the Curie depth and below which all rocks are nonmagnetic. The dominant ferromagnetic mineral in the Earth's crust is magnetite, which has a Curie temperature of 580°C (853 K) (Lanza & Meloni, 2006), so the deepest crustal magnetic source provides an estimate of the depth to the magnetite Curie depth and hence the 580°C isotherm. From this depth, geothermal heat flux at the surface can be estimated using a thermal model.

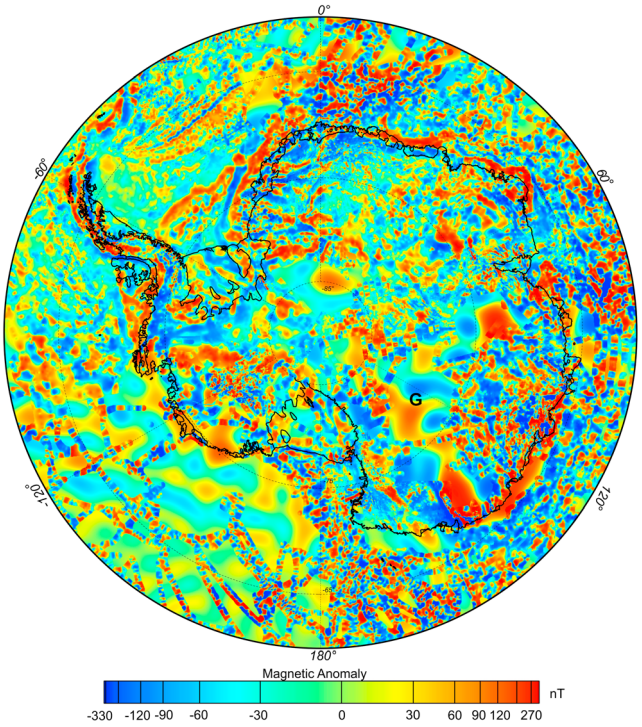

Figure 1. New magnetic anomaly compilation for Antarctica and surrounding areas. G, gap in the airborne data filled using MF7.

2.1. Magnetic Compilation

To produce our Antarctic-wide compilation of magnetic anomalies, we used (Table S1) the following: all the publicly available aeromagnetic data for the Antarctic continent and surrounding areas: ADMAP (Golynsky et al., 2001), WISE (Ferraccioli et al., 2009), AFI-Coats Land (Bamber et al., 2006), AGAP (Ferraccioli et al., 2011), PPT (Studinger et al., 2006), ICECAP (Aitken et al., 2014), Central TAM (Goodge & Finn, 2010), and Weddell Sea (Jordan et al., 2017); a reprocessed version of a compilation over Dronning Maud Land (Mieth & Jokat, 2014) and ICEGRAV2013 (Forsberg et al., 2017); and satellite magnetic data from the Magnetic Field Model MF7 (MF7) (Maus, 2010).

All magnetic anomalies from airborne surveys were upward continued (i.e., values are extrapolated to certain altitude based on a mathematical operator, Telford et al., 1990) to 5 km height and had MF7 as a reference level. The long wavelength content (>150 km) related to the maximum resolution of the satellite data was filtered from all surveys before the data were merged following the WDMAM 2.0 procedure (Catalán et al., 2016; Lesur et al., 2016). The 5 km resolution is based on the lowest resolution provided by the airborne data. Finally, the long wavelength signal from satellite data was introduced for the whole compilation and also to provide coverage in the gaps.

2.2. Curie Depth Estimate and Its Uncertainty

Magnetic anomalies are sensitive to the thermal profile of the lithosphere. Under certain conditions spectral analysis is able to determine depths of magnetic discontinuities (Spector & Grant, 1970). We take advantage of this to derive Curie depth estimates from the magnetic anomaly data. There are different techniques to estimate the base of the magnetic sources (Ravat et al., 2007). We selected the defractal spectral method (Figure S1 in the supporting information, flowchart of the procedure) as it is appropriate for regional compilations of magnetic anomalies and it has been extensively used elsewhere to estimate the Curie depth (Bouligand et al., 2009; Khojamli et al., 2017; Okubo & Matsunaga, 1994; Salem et al., 2014). All these techniques use the same approximation based on the existence of a linear relationship between the spectral power density and specific wave number ranges. This allows us to estimate the depth to the top and the depth to the centroid of the magnetic sources. To infer the Curie depth, we used a three-step procedure described in detailed in the supporting information. First, we estimate the depth to the top of the deepest magnetic body, Z_t; second, we estimate the centroid depth of the deepest magnetic body, Z_o (Figure S2). Finally, the Curie depth or depth to the bottom of the magnetic source, Z_b, is inferred by a simple mathematical relationship.

The defractal spectral method does not assume a random and uncorrelated distribution of sources, but follows a fractal/scale distribution (Bansal et al., 2011; Maus & Dimri, 1996). This considers that there is a relationship between the observed power spectral density and the power spectral density of the random magnetization model (1):

$$P_R(k_x, k_y) = P_F(k_x, k_y) \cdot k^{\alpha}, \tag{1}$$

where $P_F(k_x, k_y)$ is the observed power spectrum, $P_R(k_x, k_y)$ represents the power spectrum due to random magnetization modeling, k is referred to radial wave number, and α denotes the fractal parameter. The fractal parameter, α, is related to the fractal parameter of magnetization, β, by $\alpha = \beta - 1$.

If the fractal parameter is known, once the fractal effect of the magnetization spectrum was removed, we estimated the depth to the top, Z_t, and depth to the centroid, Z_o, of the magnetic sources following the procedure of Tanaka et al. (1999), which is known as the centroid spectral method. This is appropriate for regional compilations of magnetic anomalies and has been extensively used to estimate Curie depths (Bouligand et al., 2009; Khojamli et al., 2017; Li, 2011; Li et al., 2009, 2010; Ravat et al., 2007; Salazar et al., 2017; Salem et al., 2014; Tanaka et al., 1999; Vargas et al., 2015).

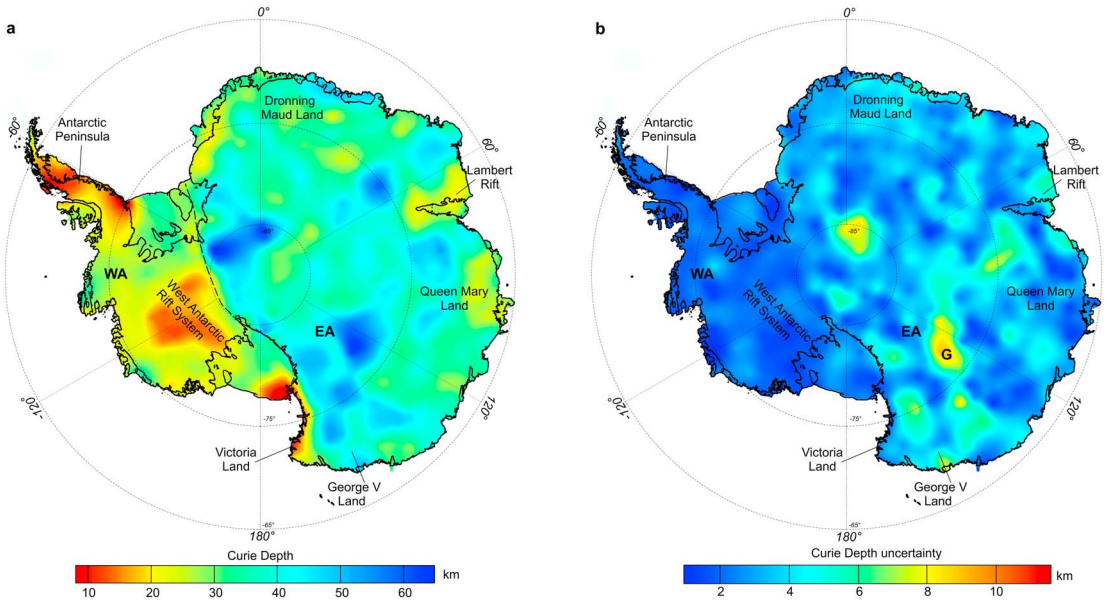

Figure 2. Curie depth and its uncertainty. (a) Curie depth map. Dashed line: boundary between East and West Antarctica considering satellite gravity, seismology, topography, and geology information. (b) Uncertainty distribution for curie depth. G, gap in the airborne data.

Once the windows size and the wave number ranges were determined (supporting information), we calculated the best fit for the fractal parameter α. This value is not known, and as it strongly correlated with the depth to the top (Bouligand et al., 2009), and there is no direct way but an iterative process to get it. We followed an iterative process where we checked different values for α and selected the best fit between the random magnetization model spectrum and the synthetic spectrum. After testing values of α ranging from 0 to 2 on 0.1 steps, we obtained the best fit between the random magnetization model spectrum and the synthetic spectrum for $\alpha = 0.2$. Values of $\alpha > 2$ over correct the spectra providing unreliable shallow Curie depths values.

Finally, we integrated our point estimates of Curie depth into 15 km resolution maps for East Antarctica (EA) and West Antarctica (WA). EA and WA were treated separately since they present different radial average power density spectra (Figure S3) due to their differences in geology and evolution (Dalziel & Elliot, 1982). The results derived for each region were then combined in one single grid along the geological and geophysical boundary observed and described by satellite gravity (Block et al., 2009), seismology (An et al., 2015b), topography (Fretwell et al., 2013), and geological data (Dalziel & Elliot, 1982) (Figure 2a).

The uncertainties in the Curie depth estimate (Figure 2b), ΔZ_b, were based on the uncertainties in fit when deriving Z_t and Z_o using the spectral method (2) and were calculated as follows:

$$\Delta Z_b = \sqrt{4\Delta {Z_o}^2 + \Delta {Z_t}^2}. \tag{2}$$

2.3. Heat Flux and Its Uncertainty

To determine the heat flux distribution over the Antarctic continent, we assume the 1-D heat conduction equation under the steady state condition, no lateral variations of properties and that heat production is considered continuous in the lithosphere and decreases exponentially with depth (Turcotte & Schubert, 2002):

$$K\frac{\partial^2 T(z)}{\partial z^2} = -H_0 e^{-(z-z_0)/h_r}, \tag{3}$$

where K is thermal conductivity, T is temperature, z is depth, H_0 is the heat production at the surface, and h_r is the scale depth.

Integrating this equation twice, we obtained the temperature profile, which is related to the heat flux:

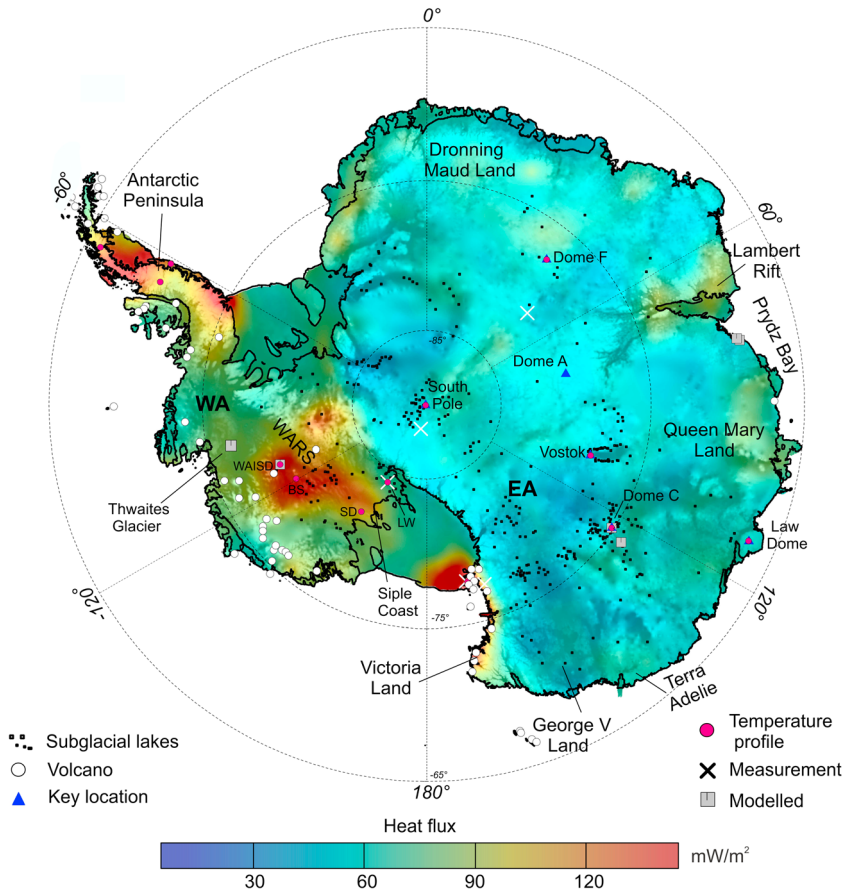

Figure 3. Geothermal heat flux distribution at the ice-rock interface superimposed on subglacial topography. Table S2 shows details of the local values. BS, Byrd Station; LW, Lake Whillans; SD, Siple dome; and WASID, West Antarctic Ice Sheet Divide.

$$q(z) = -K\frac{\partial T(z)}{\partial z}. \tag{4}$$

Assuming the boundary conditions that at the Curie depth, Z_b, the temperature is the Curie temperature, T_c (853 K), and at the bedrock (Fretwell et al., 2013), $z = Z_0$, the temperature is T_0 (273 K), we solved the equation (4) for the heat flux at the surface, in this case at the bedrock ice interface:

$$q_s = -K\frac{\partial T(z)}{\partial z}\bigg|_{z=Z_0} = -\frac{K(T_c - T_0)}{Z_b - Z_0} - H_0 h_r + \frac{H_0 h_r^2}{Z_b - Z_0}\left(1 - e^{(-(Z_b - Z_0)/h_r)}\right). \tag{5}$$

A Curie temperature of 853 K reflects the temperature at which magnetite loses its ferromagnetic properties. A bedrock temperature of 273 K (0°C) is consistent with the observation and numerical predictions of extensive hydrological system beneath the Antarctic ice sheet (Jamieson et al., 2010; Siegert et al., 2005).

The initial values for the thermal parameters were based on typical values measured in nature (Sandiford & McLaren, 2002). Representative values for the entire Antarctic continent were further optimized in this study by comparing model outputs with direct heat flux measurements (Fisher et al., 2015; Hasterok, 2010), estimates from ice temperature profiles (Price et al., 2002) and other, more indirect methodologies including ice balance and studies of ice internal structure in Antarctica (Carter et al., 2009; Raymond, 2000; Schröeder et al., 2014) (Table S2). These data are very rare in Antarctica and sometimes not very reliable due to difficulties during measuring associated with melting ice (Zagorodnov et al., 2012). Table S2 and Figure 3 show details of these data. After optimization assumed continent-wide thermal parameters were K = 2.8 W/mK, $H_0 = 2.5 \cdot 10^{-6}$ W/m^3 and h_r = 8 km.

The formal uncertainty distribution of the heat flux (Figure S4) is calculated using the propagation equation for independent uncertainties (6). These uncertainties are calculated considering a maximum range of values for the thermal parameters that play an important role in the heat equation.

$$\Delta q_s = \sqrt{\left(\frac{\partial q_s}{\partial K}\Delta K\right)^2 + \left(\frac{\partial q_s}{\partial h_r}\Delta h_r\right)^2 + \left(\frac{\partial q_s}{\partial Z_b}\Delta Z_b\right)^2}. \quad (6)$$

We considered the spatially varying uncertainties in Z_b estimates, the uncertainty contribution of considering a constant value of h_r (where Δh_r=±3 km), and the uncertainties for using a constant value for the thermal conductivity, K, which is expected to be 10 mW/m^2 (Fox Maule et al., 2005). The uncertainties related to different values of temperature at bedrock elevation are considered very small and hence neglected since most of the Antarctic continent is at 273 K or very close to this value in the rock-ice interface (Jamieson et al., 2010; Pattyn, 2010; Siegert et al., 2005). The uncertainties related to applying constant values for parameters such as K and h_r are considered primary sources of error since they are on the same order than the final estimated uncertainty (see supporting information), while the fact of considering a constant bedrock temperature is considered a secondary source of error.

3. Curie Depth and Geothermal Heat Flux Maps Description

We found that our estimated Curie depths are greater in EA than in WA, ranging from 22 to 63 km and from 8 to 32 km, respectively as expected based on seismic estimates of crustal thickness (An et al., 2015b). In EA the thicker regions are located toward the interior, while Victoria Land, George V Land, Queen Mary Land, the Lambert Rift region, and the coastal part of Dronning Maud Land are characterized by shallower Curie depths. The shallower Curie depths in WA are found in the West Antarctic Rift System and the Antarctic Peninsula. As our spectral analysis is optimized for airborne data, higher uncertainties are concentrated in areas of poor airborne coverage and gaps (Figures 1 and 2b), where the Curie depth cannot be resolved at the same resolution.

The heat flux map (Figure 3) indicates values ranging from 42 to 180 mW/m^2 with an average of 68 mW/m^2, which is close to the global continental average of 65 mW/m^2 (Pollack et al., 1993). High values (65–180 mW/m^2) are located in WA especially in the West Antarctic Rift system (maximum of 130 mW/m^2) and the Antarctic Peninsula (maximum of 170 mW/m^2). EA is characterized by low values (45–85 mW/m^2), especially in the central part. The uncertainty calculation indicates low values, around 10 mW/m^2, with small regions of higher uncertainties (Figure S4). The standard deviation is 3 mW/m^2.

4. Discussion and Model Validation

Our heat flux results are very close to or within uncertainty compared to the heat flux measurements and other heat flux estimates (Carson et al., 2014; Carter et al., 2009; Clow et al., 2012; Dahl-Jensen et al., 1999; Damiani et al., 2014; Decker & Bucher, 1982; Dmitriev et al., 2016; Engelhardt, 2004; Fisher et al., 2015; Gow et al., 1968; Hasterok, 2010; Hondoh et al., 2002; Morin et al., 2010; Nicholls & Paren, 1993; Parrenin, 2016; Price et al., 2002; Raymond, 2000; Risk & Hochstein, 1974; Ritz et al., 2010; Salamatin et al., 1998; Schröeder et al., 2014, 2011; Zagorodnov et al., 2012) (Table S2). For example, values for Vostok (Salamatin et al., 1998) and South Pole (Price et al., 2002) are calculated to be 50–56 mW/m^2 and 61 mW/m^2, respectively, while our results show values of 52 and 59 mW/m^2 for these two regions. Similar comparisons can be made for the heat flux obtained with our spectral method and values derived from ice flow/balance modeling (Raymond, 2000), analyzes of the hydrology (Schröeder et al., 2014), and airborne radar (Parrenin, 2016). Our results are in good agreement, for example, with Thwaites Glacier (Schröeder et al., 2014) and Siple Coast (Raymond, 2000), which are both characterized by high values (80–100 mW/m^2).

Our model is in agreement with previous studies (An et al., 2015a; Fox Maule et al., 2005; Shapiro & Ritzwoller, 2004) with respect to principal differences between EA and WA (Figure 4). However, we further resolve differences between the Antarctic Peninsula and the West Antarctic Rift System and show that EA exhibits higher spatial variability than previously proposed. The study by An et al. (2015a), based on seismology, indicates high heat flux observed in the western coast of WA related to a Mesozoic subduction system. Our results do not image this feature and instead show that the high heat flux is associated with the West Antarctic

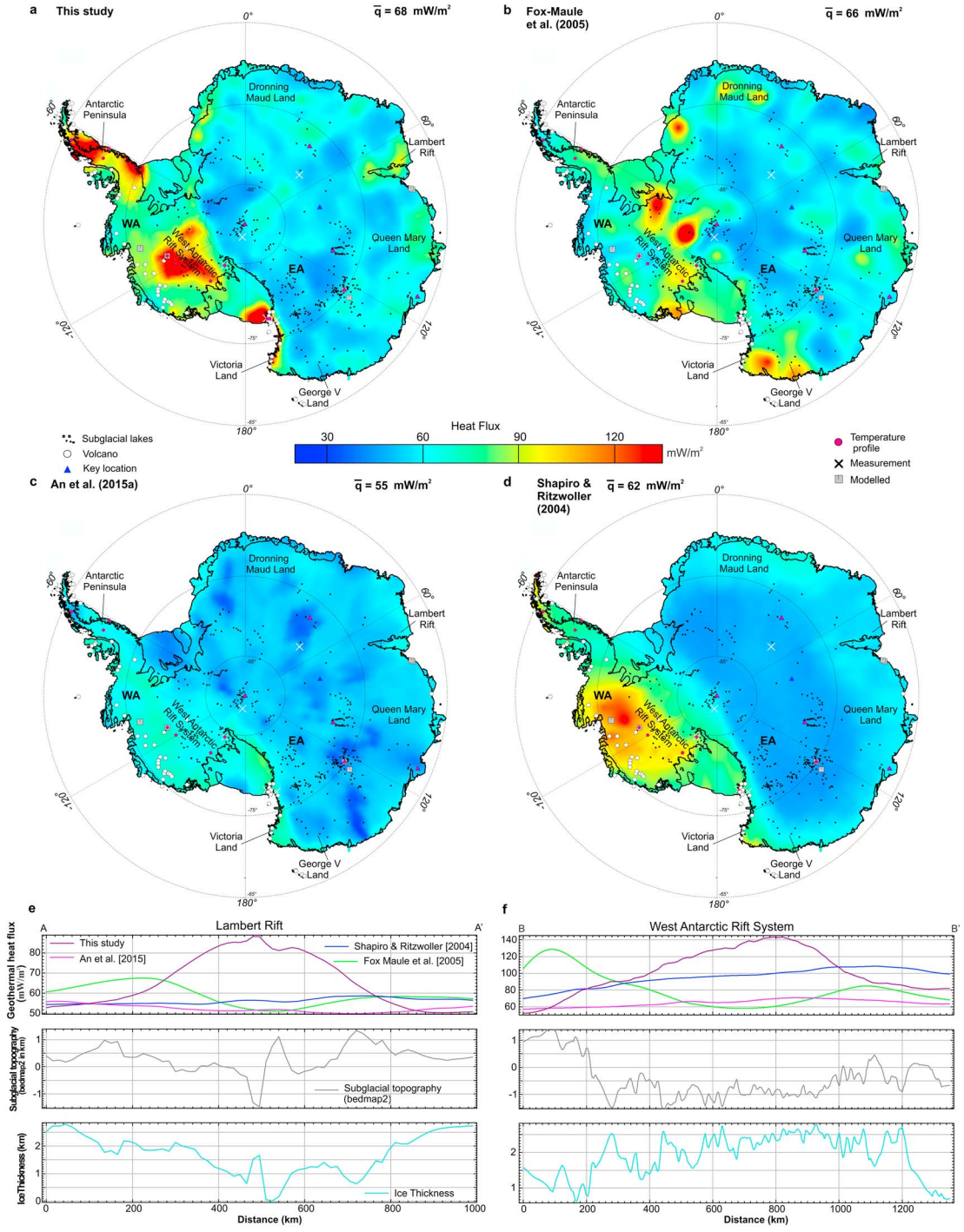

Figure 4. (a–d) Comparison of heat flux maps. (e and f) Comparisons of the four maps in the Lambert Rift and in the West Antarctic Rift System.

Rift system noted by Fox Maule et al. (2005). The differences likely result from the lower resolution of the data source and the sparse seismic stations used to calculate the Curie depth by seismology (An et al., 2015a). Direct comparison of our method with the seismic inversion is not straightforward as the seismic method is based on inversion of a mechanical model, while our method more directly estimates the depth of the thermal discontinuity. Our distribution represents the subglacial geology better than the previous one, for example, identifying high heat flux in rift systems (Golynsky & Golynsky, 2007) and volcanic regions (LeMasurier & Thomson, 1990). Figure 4 shows the differences between the four models in the Lambert Rift and the West Antarctic Rift system. Our map shows elevated heat flux in the location of the rifts, while

the other models show either a low or a flat signal. The Antarctic Peninsula shows higher spatial variability and amplitude in our study, while that is not the case in previous proposed maps. A recent model from the Antarctic Peninsula (Burton-Johnson et al., 2017) based on heat production values from rock samples and the crustal model by An et al. (2015b) has some resemblance with our map in the same region in terms of the distribution of heat flux values. Elevated heat flux is found in the eastern part of the Antarctic Peninsula, while low values are in the west and northern tip in both maps. However, the higher differences are concentrated in the central part of the Antarctic Peninsula. A local measurement of 88 mW/m^2 fits very well with our model (92 mW/m^2), while it almost double the one obtained by Burton-Johnson et al. (2017).

To check our heat flux uncertainty estimate, we have compared our results with the most complete compilation of independent sources such as local heat flux measurements (Fisher et al., 2015; Hasterok, 2010), temperature profiles (Price et al., 2002; Salamatin et al., 1998), and heat flux values derived from ice flow/balance modeling, analyzes of the hydrology, and airborne radar data in different locations of Antarctica (Carter et al., 2009; Raymond, 2000; Schröeder et al., 2014) (Table S2). Our heat flux map was calculated from representative Curie depth values derived from spectral analysis performed over multiple overlapping windows optimized for analysis of the aeromagnetic data. This means that these average heat flux values cannot strictly be compared with local measurements. Having this in mind, we discarded those local heat flux values which are far outside the expected values, even for young crust, as these most likely reflect very localized geothermal perturbations rather than the regional representative average for an area (e.g., values such as 285 mW/m^2 located in Lake Whillans). We also discarded local heat flux values located in areas with high gradient of magnetic anomaly signal, Curie depth, heat flux, and topography as they are not located in regions that are representative of the mean value of an area. Accordingly, we did not consider some of the values obtained in WA, such as some in Lake Whillans, Bird Station, Siple Dome, and West Antarctic Ice Sheet Divide. The majority of these omitted values are very high and are considered to be local anomalies. Finally, we compared the remaining local heat flux estimates with our results. We obtained a mean difference of 1.4 mW/m^2 and a standard deviation of 14 mW/m^2. Using these as representative of the precision of our heat flux map, we can compare it with our mean uncertainty estimate for these specific locations (13 mW/m^2) and the mean error budget calculated for the local values obtained through the different methodologies (13 mW/m^2). They show a reasonable agreement in support of our calculation of the uncertainty.

We carried out the same procedure of comparison between the previous proposed maps (An et al., 2015a; Fox Maule et al., 2005; Shapiro & Ritzwoller, 2004) (Figure 4) and the independent local geothermal heat flux estimates. The highest standard deviation was found for the most recent study (An et al., 2015a) (Figure 4c). Although the oldest study (Shapiro & Ritzwoller, 2004) (Figure 4d) shows the largest mean difference, the standard deviation is lower than Fox Maule et al. (2005) and An et al. (2015a) (Figures 4b and 4c), indicating the broad pattern of spatial variation is resolved. According with these statistics, our results show an internal coherency with the independent local estimates of spatial variations in geothermal heat flux between 36 and 50% better than previously proposed distributions (Table S3).

Our new map has significant value across key areas of research, including tectonics, subglacial lake distribution, subglacial hydrology, ice core site selection, and ice sheet and sea level modeling. Elevated heat flux values (~80–180 mW/m^2) are consistent with the presence of volcanic regions (LeMasurier & Thomson, 1990) and relatively recent (Mesozoic to Cenozoic) (Pollack et al., 1993) tectonic activity in WA. EA is characterized by low values (30–60 mW/m^2), as expected for a dominantly cratonic region (Dalziel & Elliot, 1982; Pollack et al., 1993). However, the coastal part of Queen Mary Land, the Lambert Rift, and Victoria Land show higher values that may provide further evidence for Cenozoic processes (Pollack et al., 1993) occurring in EA, including volcanism (LeMasurier & Thomson, 1990), uplift (Hambrey & McKelvey, 2000), or extension (Faccenna et al., 2008).

The existence and distribution of hundreds of lakes underneath the ice sheet is well known (Wright & Siegert, 2012), and studies based on thermal regime above the subglacial lakes require heat fluxes of $>$54 mW/m^2 to maintain basal ice at the pressure-melting point in the interior of EA and even higher values in coastal parts including Terra Adelie and George V Land (Siegert & Dowdeswell, 1996). Our results confirm that heat flux is high enough to support an active hydrological system. In addition, our new high-resolution heat flux map and its uncertainties will provide more precise estimates of basal temperature and the extent of melting ice at the base of the ice sheet (Van Liefferinge & Pattyn, 2013), which, in turn, will help providing more

realistic models of ice stream dynamics and improve the knowledge on subglacial hydrology distribution across the continent.

Palaeoclimate researchers are searching for optimum sites to acquire ice cores containing climate records >800,000 years old (Jouzel et al., 2007) to study the change in pacing of glacial cycles associated with the dramatic mid-Pleistocene climatic transition (Elderfield et al., 2012). Modeling to identify the best sites primarily requires knowledge of ice thickness and basal heat flux (Van Liefferinge & Pattyn, 2013). Our map provides the first regionally consistent high-resolution estimates of geothermal heat flux across all the proposed target drill sites. Generally, low values are recovered in EA but variations of up to 20% occur between the key candidate sites (Dome F (65 ± 12 mW/m^2), South Pole (59 ± 11 mW/m^2), Dome C (58 ± 12 mW/m^2), Dome A (55 ± 11 mW/m^2) and Vostok (52 ± 12 mW/m^2)), which may be significant for site selection.

Ice sheet models are crucial for estimating the Antarctic contribution to past and future global sea level changes (Golledge et al., 2015). There are two main techniques for establishing basal boundary conditions for such models. Inversion technique estimates basal conditions such as the basal traction coefficients from observed ice flow velocities (Arthern et al., 2015). The alternative forward modeling approach imposes specific parameters, including geothermal heat flux, which is the least known in terms of its spatial variability on the continent. In most ways the second approach is preferable, and our new results may make this technique more feasible.

5. Conclusions

Our method of reproducing the heat flux distribution for the Antarctic continent is 36–50% better (see section 2 and Table S3) and reproduces geological variations more reasonably than previous methods, which were based on low-resolution and/or scarce data. Also, we calculated, for first time, the uncertainty distribution. Additionally, our thermal model is the first to consider the available local values from the continent (Table S2). Our results have the potential to contribute to more realistic and precise studies of subglacial hydrology distribution, improved ice core site selection, and enhance ice sheet and sea level modeling to better reconstruct past and predict future changes.

Acknowledgments

We wish to thank the ADMAP-2 project, and specifically the Korean Polar Institute, whose support made reprocessing and integration of the new Dronning Maud Land magnetic data possible. We also wish to acknowledge René Forsberg, Fausto Ferraccioli, Marta Ghidella, and Kenny Matsuoka from the ICEGRAV 2013 project for aeromagnetic data over the Recovery Ice Stream. We thank two anonymous reviewers who helped improving the manuscript. Y. M. M. thanks the Marie Skłodowska-Curie Program from the European Commission for supporting this research. More details about data, methodology, and results can be found in the supporting information file of this article. The resulting Curie depth and geothermal heat flux models and their associated uncertainties can be found at PANGAEA (https://doi.pangaea.de/10.1594/PANGAEA.882503).

References

Aitken, A. R. A., Young, D. A., Ferraccioli, F., Betts, P. G., Greenbaum, J. S., Richter, T. G., … Siegert, M. J. (2014). The subglacial geology of Wilkes land, East Antarctica. *Geophysical Research Letters*, *41*, 2390–2400. https://doi.org/10.1002/2014GL059405

An, M., Wiens, D. A., Zhao, Y., Feng, M., Nyblade, A., Kanao, M., … Lévêque, J. J. (2015a). Temperature, lithosphere-asthenosphere boundary, and heat flux beneath the Antarctic plate inferred from seismic velocities. *Journal of Geophysical Research: Solid Earth*, *120*, 8720–8742. https://doi.org/10.1002/2015JB011917

An, M., Wiens, D. A., Zhao, Y., Feng, M., Nyblade, A. A., Kanao, M., … Lévêque, J. J. (2015b). S-velocity model and inferred Moho topography beneath the Antarctic plate from Rayleigh waves. *Journal of Geophysical Research: Solid Earth*, *120*, 359–383. https://doi.org/10.1002/2014JB011332

Arthern, R. J., Hindmarsh, R. C., & Williams, C. R. (2015). Flow speed within the Antarctic ice sheet and its controls inferred from satellite observations. *Journal of Geophysical Research: Earth Surface*, *120*, 1171–1188. https://doi.org/10.1002/2014JF003239

Bamber, J. L., Ferraccioli, F., Joughin, I., Shepherd, T., Rippin, D. M., Siegert, M. J., & Vaughan, D. G. (2006). East Antarctic ice stream tributary underlain by major sedimentary basin. *Geology*, *34*(1), 33–36. https://doi.org/10.1130/G22160.1

Bansal, A. R., Gabriel, G., Dimri, V. P., & Krawczyk, C. M. (2011). Estimation of depth to the bottom of magnetic sources by a modified centroid method for fractal distribution of sources: An application to aeromagnetic data in Germany. *Geophysics*, *76*(3), L11–L22. https://doi.org/10.1190/1.3560017

Block, A. E., Bell, R. E., & Studinger, M. (2009). Antarctic crustal thickness from satellite gravity: Implications for the transantarctic and Gamburtsev Subglacial Mountains. *Earth and Planetary Science Letters*, *288*, 194–203.

Bouligand, C., Glen, J. M. G., & Blakely, R. J. (2009). Mapping curie temperature depth in the western United States with a fractal model for crustal magnetisation. *Journal of Geophysical Research*, *114*, B11104. https://doi.org/10.1029/2009JB006494

Burton-Johnson, A., Halpin, J. A., Whittaker, J. M., Graham, F. S., & Watson, S. J. (2017). A new heat flux model for the Antarctic Peninsula incorporating spatially variable upper crustal radiogenic heat production. *Geophysical Research Letters*, *44*, 5436–5446. https://doi.org/10.1002/2017GL073596

Carson, C. J., McLaren, S., Roberts, J. L., Boger, S. D., & Blankenship, D. D. (2014). Blankenship, hot rocks in a cold place: High sub-glacial heat flow in East Antarctica. *Journal of the Geological Society of London*, *171*(1), 9–12. https://doi.org/10.1144/jgs2013-030

Carter, S. P., Blankenship, D. D., Young, D. A., & Holt, J. W. (2009). Using radar-sounding data to identify the distribution and sources of subglacial water: Application to dome C, East Antarctica. *Journal of Glaciology*, *55*(194), 1025–1040. https://doi.org/10.3189/002214309790794931

Catalán, M., Dyment, J., Choi, Y., Hamoudi, M., Lesur, V., Thébault, E., … Taylor, P. (2016). Making a better magnetic map. *Eos*, *97*. https://doi.org/10.1029/2016EO054645

Clow, G. D., Cuffey, K. M., & Waddington, E. D. (2012). High heat-flow beneath the central portion of the West Antarctic Ice Sheet. Abstract C31A-0577 Presented at the 2012 AGU Fall Meeting, San Francisco, CA.

Dahl-Jensen, D., Morgan, V. I., & Elcheikh, A. (1999). Monte Carlo inverse modelling of the law dome (Antarctica) temperature profile. *Annals of Glaciology*, *29*, 145–150. https://doi.org/10.3189/172756499781821102

Dalziel, I. W., & Elliot, D. H. (1982). West Antarctica: Problem child of Gondwanaland. *Tectonics*, *1*(1), 3–19. https://doi.org/10.1029/TC001i001p00003

Damiani, T. M., Jordan, T. A., Ferraccioli, F., Young, D. A., & Blankenship, D. D. (2014). Variable crustal thickness beneath Thwaites glacier revealed from airborne gravimetry, possible implications for geothermal heat flux in West Antarctica. *Earth and Planetary Science Letters*, *407*, 109–122. https://doi.org/10.1016/j.epsl.2014.09.023

Decker, E. R., & Bucher, G. J. (1982). Geothermal studies in the Ross Island-Dry Valley region. *Antarct Geoscience*, *4*, 887–894.

Dmitriev, A. N., Bolshunov, A. V., & Podoliak, A. V. (2016). Assessment of ice borehole temperature conditions at interface with subglacial Lake Vostok (Antarctica). *International Journal of Applied Engineering Research*, *11*, 7230–7233.

Elderfield, H., Ferretti, P., Greaves, M., Crowhurst, S., McCave, I. N., Hodell, D., & Piotrowski, A. M. (2012). Evolution of ocean temperature and ice volume through the mid-Pleistocene climate transition. *Science*, *337*(6095), 704–709. https://doi.org/10.1126/science.1221294

Engelhardt, H. (2004). Ice temperature and high geothermal flux at Siple Dome, West Antarctica, from borehole measurements. *Journal of Glaciology*, *50*(169), 251–256. https://doi.org/10.3189/172756504781830105

Faccenna, C., Rossetti, F., Becker, T. W., Danesi, S., & Morelli, A. (2008). Recent extension driven by mantle upwelling beneath the Admiralty Mountains (East Antarctica). *Tectonics*, *27*, TC4015. https://doi.org/10.1029/2007TC002197

Ferraccioli, F., Armadillo, A., Jordan, T. A., Bozzo, E., & Corr, H. (2009). Aeromagnetic exploration over the East Antarctic ice sheet: A new view of the Wilkes Subglacial Basin. *Tectonophysics*, *478*(1-2), 62–77. https://doi.org/10.1016/j.tecto.2009.03.013

Ferraccioli, F., Finn, C. A., Jordan, T. A., Bell, R. E., Anderson, L. M., & Damaske, D. (2011). East Antarctic rifting triggers uplift of the Gamburtsev Mountains. *Nature*, *479*(7373), 388–392. https://doi.org/10.1038/nature10566

Fisher, A. T., Mankoff, K. D., Tulaczyk, S. M., Tyler, S. W., & Foley, N. (2015). High geothermal heat flux measured below the West Antarctic ice sheet. *Science Advances*, *1*(6), e1500093. https://doi.org/10.1126/sciadv.1500093

Forsberg, R., Olesen, A. V., Ferraccioli, F., Jordan, T. A., Matsuoka, K., Zakrajsek, A., … Greenbaum, J. S. (2017). Exploring the Recovery Lakes region and interior Dronning Maud land, East Antarctica, with airborne gravity, magnetic and radar measurements. In *Exploration of subsurface Antarctica: Uncovering past changes and modern processes*. *Geological Society of London, Special Publications, 461*. https://doi.org/10.1144/SP461.17

Fox Maule, C., Purucker, M. E., Olsen, N., & Mosegaard, K. (2005). Heat flux anomalies in Antarctica revealed by satellite magnetic data. *Science*, *309*(5733), 464–467. https://doi.org/10.1126/science.1106888

Fretwell, P., Pritchard, H. D., Vaughan, D. G., Bamber, J. L., Barrand, N. E., Bell, R., … Zirizzotti, A. (2013). Bedmap2: Improved ice bed, surface and thickness datasets for Antarctica. *The Cryosphere*, *7*(1), 375–393. https://doi.org/10.5194/tc-7-375-2013

Golledge, N. R., Kowalewski, D. E., Naish, T. R., Levy, R. H., Fogwill, C. J., & Gasson, E. G. W. (2015). The multi-millennial Antarctic commitment to future sea-level rise. *Nature*, *526*(7573), 421–425. https://doi.org/10.1038/nature15706

Golynsky, D. A., & Golynsky, A. V. (2007). Gaussberg rift—Illusion or reality? 10th international symposium on Antarctic earth sciences, Extended Abstract, 168.

Golynsky, A., Chiappini, M., Damaske, D., Ferraccioli, F., Ferris, J., Finn, C., … Torta, M. (2001). ADMAP—Magnetic anomaly map of the Antarctic, 1:10 000 000 scale map. In P. Morris & R. R. B. von Frese (Eds.), *British Antarctic Survey Misc* (Vol. 10). Cambridge: British Antarctic Survey.

Goodge, J. W., & Finn, C. A. (2010). Glimpses of East Antarctica: Aeromagnetic and satellite magnetic view from the central Transantarctic Mountains of East Antarctica. *Journal of Geophysical Research*, *115*, B09103. https://doi.org/10.1029/2009JB006890

Gow, A. J., Ueda, H. T., & Garfield, D. E. (1968). Antarctic ice sheet: Preliminary results of first core hole to bedrock. *Science*, *161*(3845), 1011–1013. https://doi.org/10.1126/science.161.3845.1011

Hambrey, M. J., & McKelvey, B. (2000). Major Neogene fluctuations of the East Antarctic ice sheet: Stratigraphic evidence from the Lambert glacier region. *Geology*, *28*(10), 887–890. https://doi.org/10.1130/0091-7613(2000)28%3C887:MNFOTE%3E2.0.CO;2

Hasterok, D. (2010). Thermal state of continental and oceanic lithosphere, PhD thesis, 167 pp. University of Utah.

Hondoh, T., Shoji, H., Watanabe, O., Salamatin, A. N., & Lipenkov, V. Y. (2002). Depth-age and temperature prediction at dome Fuji station, East Antarctica. *Annals of Glaciology*, *35*, 384–390. https://doi.org/10.3189/172756402781817013

Jamieson, S. S. R., Sugden, D. E., & Hulton, N. R. J. (2010). The evolution of the sub-glacial landscape of Antarctica. *Earth and Planetary Science Letters*, *293*(1-2), 1–27. https://doi.org/10.1016/j.epsl.2010.02.012

Jordan, T. A., Leat, P. T., & Ferraccioli, F. (2017). New geophysical compilations link crustal block motion to Jurassic extension and strike-slip faulting in the Weddell Sea Rift system of West Antarctica. *Gondwana Research*, *42*, 29–48. https://doi.org/10.1016/j.gr.2016.09.009

Jouzel, J., Masson-Delmotte, V., Cattani, O., Dreyfus, G., Falourd, S., Hoffmann, G., … Wolff, E. W. (2007). Orbital and millennial Antarctic climate variability over the past 800,000 years. *Science*, *317*(5839), 793–796. https://doi.org/10.1126/science.1141038

Khojamli, A., Ardejani, F. D., Moradzadeh, A., Kalate, A. N., Kahoo, A. R., & Porkhial, S. (2017). Determining fractal parameter and depth of magnetic sources for Ardabil geothermal area using aeromagnetic data by de-fractal approach. *Journal of Mining and Environment*, *8*(1), 93–101.

Lanza, R., & Meloni, A. (2006). *The Earth's Magnetism*. Berlin Heidelberg: Springer-Verlag.

LeMasurier, W. E., & Thomson, J. W. (Eds.) (1990). Volcanoes of the Antarctic plate and Southern Oceans. In *Antarctic Research Series* (Vol. 48, pp. 487). Washington, DC: American Geophysical Union.

Lesur, V., Hamoudi, M., Choi, Y., Dyment, J., & Thébault, E. (2016). Building the second version of the world digital magnetic anomaly map (WDMAM). *Earth, Planets and Space*, *68*, 1–13.

Li, C.-F. (2011). An integrated geodynamic model of the Nankai subduction zone and neighboring regions from geophysical inversion and modeling. *Journal of Geodynamics*, *51*(1), 64–80. https://doi.org/10.1016/j.jog.2010.08.003

Li, C.-F., Chen, B., & Zhou, Z. (2009). Deep crustal structures of eastern China and adjacent seas revealed by magnetic data. *Science China*, *52*(Ser. D), 984–993.

Li, C.-F., Shi, X., Zhou, Z., Li, J., Geng, J., & Chen, B. (2010). Depths to the magnetic layer bottom in the South China Sea area and their tectonic implications. *Geophysical Journal International*, *182*(3), 1229–1247. https://doi.org/10.1111/j.1365-246X.2010.04702.x

Maus, S. (2010). Magnetic field model MF7.

Maus, S., & Dimri, V. (1996). Depth estimation from the scaling power spectrum of potential fields? *Geophysical Journal International*, *124*(1), 113–120. https://doi.org/10.1111/j.1365-246X.1996.tb06356.x

Mieth, M., & Jokat, W. (2014). New aeromagnetic view of the geological fabric of southern Dronning Maud land and coats land, East Antarctica. *Gondwana Research*, *25*(1), 358–367. https://doi.org/10.1016/j.gr.2013.04.003

Morin, R. H., Williams, T., Henrys, S. A., Magens, D., Niessen, F., & Hansaraj, D. (2010). Heat flow and hydrologic characteristics at the AND-1B borehole, ANDRILL McMurdo ice shelf project, Antarctica. *Geosphere*, *6*(4), 370–378. https://doi.org/10.1130/GES00512.1

Nicholls, K. W., & Paren, J. G. (1993). Extending the Antarctic meteorological record using ice-sheet temperature profiles. *Journal of Climate*, *6*(1), 141–150. https://doi.org/10.1175/1520-0442(1993)006%3C0141:ETAMRU%3E2.0.CO;2

Okubo, Y., & Matsunaga, T. (1994). Curie point depth in northeast Japan and its correlation with regional thermal structure and seismicity. *Journal of Geophysical Research*, *99*(B11), 22,363–22,371. https://doi.org/10.1029/94JB01336

Parrenin, F. (2016). *Is there 1 million-year old ice near Dome C, Antarctica?* Abstract retrieved from Abstract, Submission ID 2, International Partnerships in Ice Core Sciences, 2nd Open Science Conference, Hobart, Australia, 7-11 March 2016.

Pattyn, F. (2010). Antarctic subglacial conditions inferred from a hybrid ice sheet/ice stream model. *Earth and Planetary Science Letters*, *295*(3-4), 451–461. https://doi.org/10.1016/j.epsl.2010.04.025

Pollack, H. N., Hurter, S. J., & Johnson, J. R. (1993). Heat flow from the Earth's interior: Analysis of the global data set. *Reviews of Geophysics*, *31*(3), 267–280. https://doi.org/10.1029/93RG01249

Price, P. B., Nagornov, O. V., Bay, R., Chirkin, D., He, Y., Miocinovic, P., … Zagorodnov, V. (2002). Temperature profile for glacial ice at the south pole: Implications for life in a nearby subglacial lake. *Proceedings of the National Academy of Sciences of the United States of America*, *99*(12), 7844–7847. https://doi.org/10.1073/pnas.082238999

Ravat, D., Pignatelli, A., Nicolosi, I., & Chiappini, M. (2007). A study of spectral methods of estimating the depth to the bottom of magnetic sources from near-surface magnetic anomaly data. *Geophysical Journal International*, *169*(2), 421–434. https://doi.org/10.1111/j.1365-246X.2007.03305.x

Raymond, C. F. (2000). Energy balance of ice streams. *Journal of Glaciology*, *46*(155), 665–674. https://doi.org/10.3189/172756500781832701

Risk, G. F., & Hochstein, M. P. (1974). Heat flow at arrival heights, Ross Island, Antarctica, new zeal. *Journal of Geology and Geophysics*, *17*(3), 629–644. https://doi.org/10.1080/00288306.1973.10421586

Ritz, C., Lefebvre, E., Dahl Jensen, D., Johnsen, S., & Sheldon, S. (2010). Temperature profile measurement in the EPICA dome C borehole, EPICA meeting 2010.

Salamatin, A. N., Lipenkov, V. Y., Barkov, N. I., Jouzel, J., Petit, J. R., & Raynaud, D. (1998). Ice core age dating and paleothermometer calibration based on isotope and temperature profiles from deep boreholes at Vostok Station (East Antarctica). *Journal of Geophysical Research*, *103*(D8), 8963–8977. https://doi.org/10.1029/97JD02253

Salazar, J. M., Vargas, C. A., & Leon, H. (2017). Curie point depth in the SW Caribbean using the radially averaged spectra of magnetic anomalies. *Tectonophysics*, *694*, 400–413. https://doi.org/10.1016/j.tecto.2016.11.023

Salem, A., Green, C., Ravat, D., Hemant, K., East, P., Fairhead, J. D., … Biegert, E. (2014). Depth to curie temperature across the central Red Sea from magnetic data using the de-fractal method. *Tectonophysics*, *624-625*, 75–86. https://doi.org/10.1016/j.tecto.2014.04.027

Sandiford, M., & McLaren, S. (2002). Tectonic feedback and the ordering of heat producing elements within the continental lithosphere. *Earth and Planetary Science Letters*, *204*(1-2), 133–150. https://doi.org/10.1016/S0012-821X(02)00958-5

Schröder, H., Paulsen, T., & Wonik, T. (2011). Thermal properties of the AND-2A borehole in the southern Victoria Land Basin, McMurdo sound, Antarctica. *Geosphere*, *7*(6), 1324–1330. https://doi.org/10.1130/GES00690.1

Schröeder, D. M., Blankenship, D. D., Young, D. A., & Quartini, E. (2014). Evidence for elevated and spatially variable geothermal flux beneath the West Antarctic ice sheet. *Proceedings of the National Academy of Sciences of the United States of America*, *111*(25), 9070–9072. https://doi.org/10.1073/pnas.1405184111

Shapiro, N. M., & Ritzwoller, M. H. (2004). Inferring surface heat flux distributions guided by a global seismic model: Particular application to Antarctica. *Earth and Planetary Science Letters*, *223*(1-2), 213–224. https://doi.org/10.1016/j.epsl.2004.04.011

Siegert, M. J., & Dowdeswell, J. A. (1996). Spatial variations in heat at the base of the Antarctic ice sheet from analysis of the thermal regime above subglacial lakes. *Journal of Glaciology*, *42*(142), 501–509. https://doi.org/10.1017/S0022143000003488

Siegert, M. J., Carter, S., Tabacco, I. E., Popov, S., & Blankenship, D. D. (2005). A revised inventory of Antarctic subglacial lakes. *Antarctic Science*, *17*(03), 453–460. https://doi.org/10.1017/S0954102005002889

Spector, A., & Grant, F. S. (1970). Statistical model for interpreting aeromagnetic data. *Geophysics*, *35*(2), 293–302. https://doi.org/10.1190/1.1440092

Studinger, M., Bell, R. E., Fitzgerald, P. G., & Buck, W. R. (2006). Crustal architecture of the Transantarctic Mountains between the Scott and Reedy glacier region and south pole from aerogeophysical data. *Earth and Planetary Science Letters*, *250*(1-2), 182–199. https://doi.org/10.1016/j.epsl.2006.07.035

Tanaka, A., Okubo, Y., & Matsubayashi, O. (1999). Curie point depth based on spectrum analysis of the magnetic anomaly data in east and Southeast Asia. *Tectonophysics*, *306*(3-4), 461–470. https://doi.org/10.1016/S0040-1951(99)00072-4

Telford, W. M., Telford, W. M., Geldart, L. P., & Sheriff, R. E. (1990). *Applied geophysics* (p. 1). Cambridge: Cambridge University Press.

Turcotte, D. L., & Schubert, G. (2002). *Geodynamics* (456 pp.). Cambridge: Cambridge University Press. https://doi.org/10.1017/CBO9780511807442

Van Liefferinge, B., & Pattyn, F. (2013). Using ice-flow models to evaluate potential sites of million year-old ice in Antarctica. *Climate of the Past*, *9*(5), 2335–2345. https://doi.org/10.5194/cp-9-2335-2013

Vargas, C. A., Idarraga-Garcia, J., & Salazar, J. M. (2015). Curie point depths in northwestern South America and the southwestern Caribbean Sea. In C. Bartolini, & P. Mann (Eds.), *Petroleum geology and potential of the Colombian Caribbean margin* (Vol. 108, pp. 179–200). Tulsa, OK: AAPG Memoir. https://doi.org/10.1306/13531936M1083642

Wright, A., & Siegert, M. A. (2012). Fourth inventory of Antarctic subglacial lakes. *Antarctic Science*, *24*(06), 659–664. https://doi.org/10.1017/S095410201200048X

Zagorodnov, V., Nagornov, O., Scambos, T. A., Muto, A., Mosley-Thompson, E., Pettit, E. C., & Tyuflin, S. (2012). Borehole temperatures reveal details of 20th century warming at Bruce Plateau, Antarctic Peninsula. *The Cryosphere*, *6*(3), 675–686. https://doi.org/10.5194/tc-6-675-2012